Available online at www.sciencedirect.com
SCIENCE DIRECT®
Polyhedron 24 (2005) 2894–2899
POLYHEDRON
www.elsevier.com/locate/poly

Single-molecule magnets: synthesis, structures and magnetic properties of Mn_{11} and Mn_{25} clusters

Muralee Murugesu [a], Wolfgang Wernsdorfer [b], Khalil A. Abboud [a], George Christou [a,*]

[a] *Department of Chemistry, University of Florida, Gainesville, FL 32611-7200, USA*
[b] *Laboratoire Louis Néel-CNRS, BP 166, 25 Avenue des Martyrs, 38042 Grenoble, Cedex 9, France*

Received 8 October 2004; accepted 25 March 2005
Available online 19 May 2005

Abstract

The synthesis and structural characterization of two new manganese complexes $[Mn_{11}O_2(OH)_2(nmpd)(pdmH)_5(pdm)_5Cl_6]\cdot 4MeCN$ (**1**; $Mn^{III}_7Mn^{II}_4$; $nmpdH_2$ = 2-nitro-2-methyl-1,3-propanediol) and $[Mn_{25}O_{18}(OH)_2(N_3)_{12}(pdm)_6(pdmH)_6]Cl_2\cdot 12MeCN$ (**2**; $Mn^{IV}Mn^{III}_{18}Mn^{II}_6$; $pdmH_2$ = pyridine-2,6-dimethanol) are presented, together with a study of their magnetic properties. Complex **1** possesses a ground-state spin value of $S = 10$, whereas that for **2** is $S = 51/2$. Both complexes are new additions to the family of single-molecule magnets, displaying magnetization versus DC field hysteresis at temperatures below 0.7 K.

Keywords: Manganese; Single-molecule magnet; Cluster; Hysteresis; X-ray structure

1. Introduction

The synthesis of large cluster-aggregates has been of interest not only for their aesthetic beauty but also for their unusual physical and magnetic properties. In particular, the attainment of species with large spin ground states and large magnetoanisotropy is currently the focus of much research in the area of single-molecule magnetism [1]. Such molecules derive their properties from a combination of a large ground state spin (S) value and an Ising (or easy-axis) type of magnetoanisotropy (negative zero-field splitting parameter, D). Single-molecule magnets (SMMs) thus represent a molecular approach to nanoscale magnetic materials. Furthermore, they straddle the classical/quantum interface by also displaying quantum tunneling of magnetization (QTM) [2–19].

Manganese carboxylate chemistry has been the main source of new SMMs during the last several years [2–19], and one of our research objectives has thus been to develop new synthetic approaches to Mn clusters of various nuclearities and structural types. With this in mind, we have been exploring the simultaneous use of two different types of chelates in reaction systems in order to generate new core topologies. In earlier work, we showed how the tridentate (N,O,O) chelate pyridine-2,6-dimethanol ($pdmH_2$) provided access to $[Mn_4(O_2CMe)_2(pdmH)_6]^{2+}$ with $S = 9$ [3,4], and $[Mn_9(O_2CEt)_{12}(pdm)(pdmH)_2(L)_2]$ with $S = 11/2$ [9], both of which are SMMs. As an extension to this work, we have recently been exploring reactions with $pdmH_2$ in combination with other potential chelates such as 2-nitro-2methyl-1,3-propanediol ($nmpdH_2$), or potential bridging ligands such as azide (N_3^-). We herein report the results of this study, which has produced new Mn_{11} and Mn_{25} clusters.

* Corresponding author. Tel.: +1 352 392 6737; fax: +1 352 392 8757.
E-mail addresses: christou@chem.ufl.edu, polyhedron@chem.ufl.edu (G. Christou).

0277-5387/$ - see front matter © 2005 Elsevier Ltd. All rights reserved.
doi:10.1016/j.poly.2005.03.017

2. Experimental

2.1. Compound preparations

All manipulations were performed under aerobic conditions using materials and solvents as received.

2.1.1. $[Mn_{11}O_2(OH)_2(nmpd)(pdmH)_5(pdm)_5Cl_6]\cdot 4MeCN$ (1)

Treatment of a solution of $MnCl_2\cdot 4H_2O$ (0.75 mmol, 0.15 g), $pdmH_2$ (2.5 mmol, 0.34 g) and $nmpdH_2$ (0.75 mmol, 0.10 g) in a mixture of MeCN/MeOH (35 mL/5 mL) with one equivalent of NMe_4OH (0.25 mmol, 0.10 mL) results in the formation of a dark brown solution. This was allowed to stand undisturbed for two days, and during this time large, needle-shaped brown crystals slowly crystallized of a material identified by crystallography as $[Mn^{III}_7Mn^{II}_4O_2(OH)_2(nmpd)(pdmH)_5(pdm)_5Cl_6]\cdot 4MeCN$ ($\mathbf{1}\cdot 4MeCN$). These crystals were isolated by filtration in 64% yield. *Anal*. Calc. for dried (**1**): C, 38.17; H, 4.45; N, 5.44. Found: C, 38.29; H, 4.68; N, 5.69%.

2.1.2. $[Mn_{25}O_{18}(OH)_2(N_3)_{12}(pdm)_6(pdmH)_6]Cl_2\cdot 12MeCN$ (2)

A stirred, pale brown slurry of $MnCl_2\cdot 4H_2O$ (0.75 mmol, 0.15 g), $pdmH_2$ (2.5 mmol, 0.34 g) and NaN_3 (2.5 mmol, 0.16 g) in MeCN/MeOH (20 mL/10 mL) was treated with NMe_4OH (0.25 mmol, 0.10 mL). This resulted in a dark brown solution, which was allowed to stand undisturbed for a few weeks during which time $[Mn^{IV}Mn^{III}_{18}Mn^{II}_6O_{18}(OH)_2(N_3)_{12}(pdm)_6(pdmH)_6]Cl_2\cdot 12MeCN$ ($\mathbf{2}\cdot 12MeCN$) slowly crystallized. The black crystals were isolated in ~30% yield. *Anal*. Calc. for dried (**2**): C, 25.72; H, 2.36; N, 17.14. Found: C, 26.01; H, 2.68; N, 17.15%.

3. Results and discussion

3.1. Structural description of $[Mn_{11}O_2(OH)_2(nmpd)(pdmH)_5(pdm)_5Cl_6]\cdot 4MeCN$ ($\mathbf{1}\cdot 4MeCN$)

A labeled ORTEP plot and the central core of **1** are presented in Figs. 1 and 2, respectively. Complex $\mathbf{1}\cdot 4MeCN$ crystallizes in the monoclinic space group $P2_1/c$ with the asymmetric unit consisting of the cluster and four molecules of acetonitrile. The cluster is trapped-valence $Mn^{III}_7Mn^{II}_4$ and has an unusual undecanuclear cage structure, with seven central manganese ions (Mn3, Mn4, Mn5, Mn6, Mn7, Mn8, Mn9) held together by two μ_4-O atoms (O13, O8). Two dinuclear Mn^{III}–Mn^{II} units (Mn2–Mn1, Mn10–Mn11) are linked to each end of the Mn_7 core via μ_3-alkoxide oxygen atoms (O4, O18) provided by pdm ligands. Furthermore, two hydroxide ions (O5, O17) and alkoxide

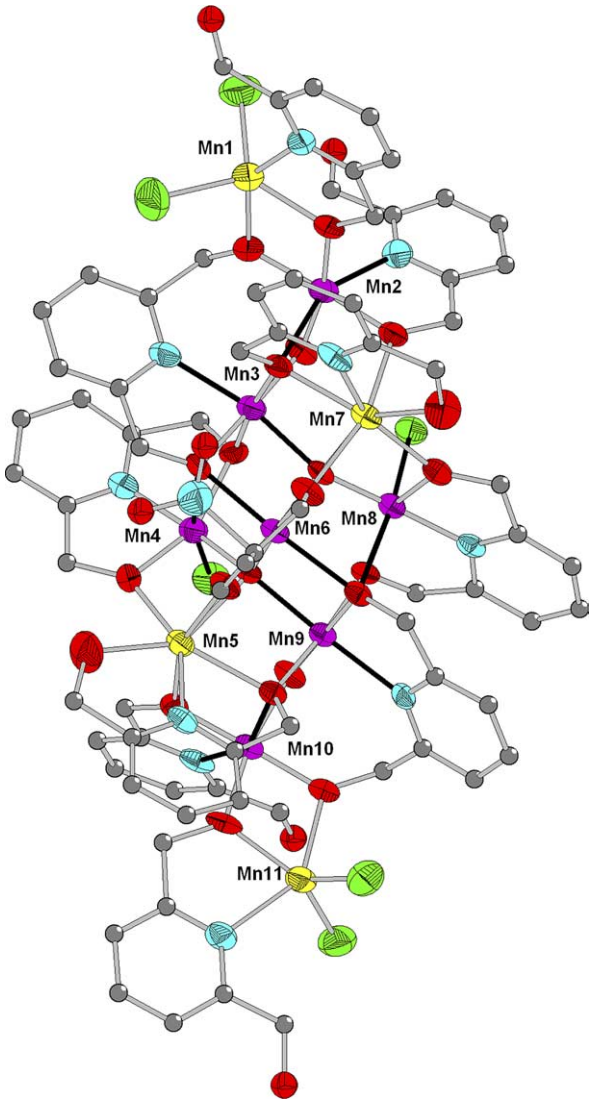

Fig. 1. ORTEP representation at the 50% probability level of complex **1**. All H atoms have been removed for clarity. Color code: purple, Mn^{III}; yellow, Mn^{II}; pale green, Cl; red, O; blue, N; gray, C.

oxygen atoms (O1, O2, O3, O7, O9, O10, O11, O12, O13, O15, O16, O19, O21, O22) from pdm and nmpd ligands provide additional bridges between the Mn ions. The coordination spheres of the Mn ions are completed by N atoms from pdm groups and six terminal Cl^- ions. The hydroxide oxygen atoms (O5 and O17), as well as the uncoordinated oxygen atoms (O25, O26, O27 and O28) are protonated, as confirmed by bond valence sum calculations; their H atoms were included in calculated, idealized positions and were refined riding on their parent atoms.

Inspection of the bond distances and bond valence sum calculations reveal that the Mn(2), Mn(3), Mn(4), Mn(6), Mn(8), Mn(9) and Mn(10) are in oxidation state Mn^{III} while the remainder of the metal ions are Mn^{II} (Figs. 1 and 2). All Mn^{III} centers display Jahn–Teller (JT) distortions as expected for high spin d^4 ions in near

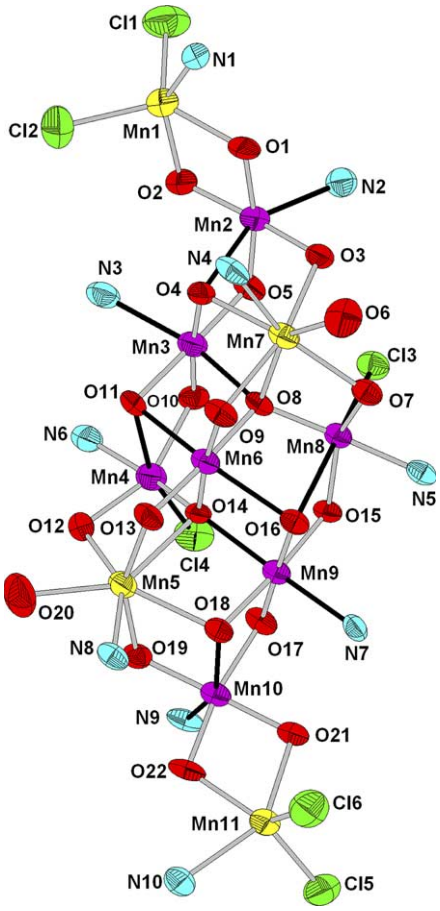

Fig. 2. Labeled ORTEP representation of the central core of complex **1**. JT axes are indicated as solid black bonds.

octahedral geometry. These take the form of axial elongations, and the JT axes are indicated as solid black bonds in Figs. 1 and 2. A close look at the crystal packing reveals no evidence of intermolecular hydrogen bonding interactions between molecules; however, intermolecular pi-stacking interactions involving the phenyl rings of pdm^{2-} ligands from neighboring Mn_{11} clusters are observed.

3.2. Structural description of $[Mn_{25}O_{18}(OH)_2(N_3)_{12}(pdm)_6(pdmH)_6]Cl_2 \cdot 12MeCN$ (**2**)

Complex **2** crystallizes in the triclinic space group $P\bar{1}$. The Mn_{25} cation lies on an inversion center and has a barrel-like structure (Fig. 3). Inspection of the structural features reveals twelve μ_4-O^{2-}, six μ_3-O^{2-} and two μ_3-OH^- ions holding the core together, as well as chelating/bridging pdm^{2-}/$pdmH^-$, and both terminal and bridging N_3^- groups. The metal oxidation states and the protonation levels of O^{2-}, OH^-, pdm^{2-} and $pdmH^-$ O atoms were established by Mn and O bond valence sum calculations, inspection of metric parameters, and detection of Mn^{III} JT elongation axes. The core of the cation may be dissected into five parallel layers of three types with an **ABCBA** arrangement (Fig. 4). Layer **A** is a Mn^{II}_3 triangular unit (Mn1, Mn2, Mn4) with a capping μ_3-OH^- ion; layer **B** is a Mn^{III}_6 triangle (Mn3, Mn5, Mn6, Mn7, Mn8, Mn9) that can be described as three corner sharing Mn^{III} triangles; and layer **C** consists of a Mn^{III}_6 hexagon (Mn11, Mn12, Mn13, Mn11a, Mn12a, Mn13a) in the center

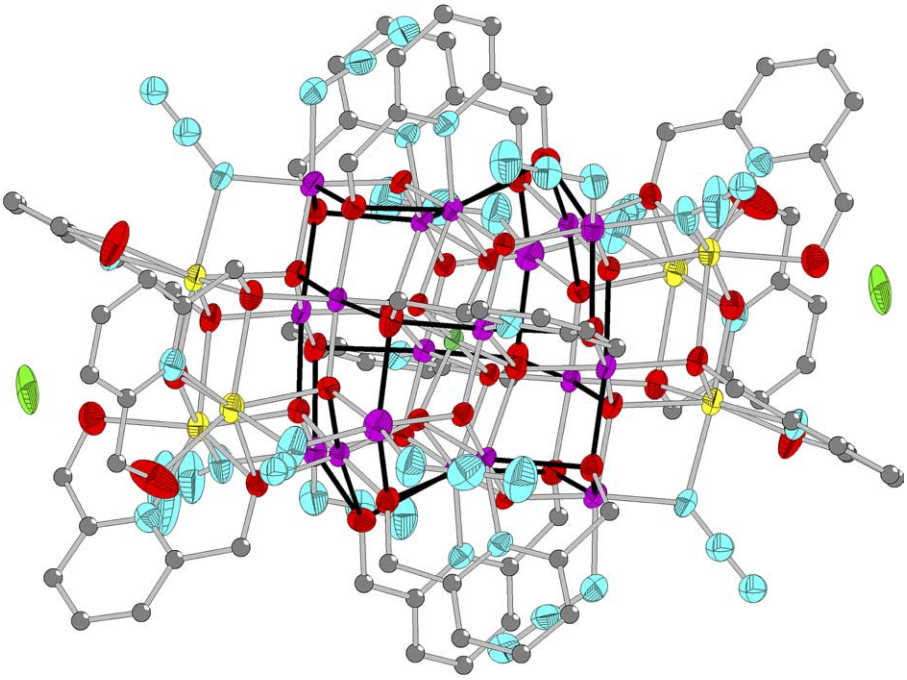

Fig. 3. ORTEP representation at the 50% probability level of the centrosymmetric complex **2**. H atoms have been removed for clarity. Color code: green, Mn^{IV}; purple, Mn^{III}; yellow, Mn^{II}; pale green, Cl; red, O; blue, N; gray, C.

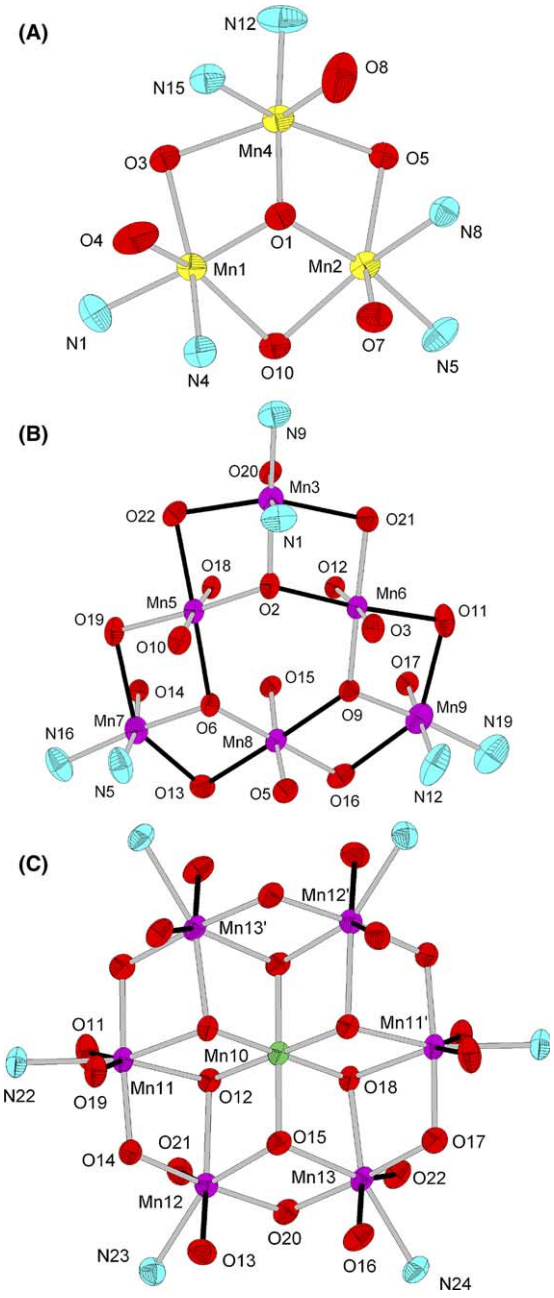

Fig. 4. Three types of constituent layers of the centrosymmetric complex **2**, color coded for clarity. Atom color code: green, Mn^{IV}; purple, Mn^{III}; yellow, Mn^{II}; red, O; blue, N. JT axes are indicated as solid black bonds.

of which is held the Mn^{IV} ion (Mn10) by the bridging O^{2-} ions. Layer **C** is reminiscent of the well known Anderson-type structure seen in some Mn complexes [20]. Each layer is linked to its neighboring layers by a combination of oxide, alkoxide and/or azide bridging groups. The outer coordination shell is occupied by pdm^{2-}, $pdmH^{-}$ and terminal azide ligands (Fig. 3). In addition, inspection of the crystal packing reveals no evidence of intermolecular hydrogen-bonding interactions between molecules.

3.3. Magnetochemistry

3.3.1. DC Magnetic susceptibility

The magnetic properties of **1** and **2** were investigated by solid state magnetic susceptibility (χ_M) measurements in the 5.0–300 K range in a DC field of 1000 Oe (0.1 Tesla); the resulting data are shown in Figs. 5 and 6, respectively, as $\chi_M T$ versus T plots. For complex **1**, the $\chi_M T$ value increases steadily from 40.2 $cm^3\,K\,mol^{-1}$ at 300 K to a maximum of 48.3 $cm^3\,K\,mol^{-1}$ at 25 K, before dropping rapidly to 40.2 $cm^3\,K\,mol^{-1}$ at 5 K. For complex **2**, the $\chi_M T$ value steadily increases from 88.4 $cm^3\,K\,mol^{-1}$ at 300 K to a maximum of 310 $cm^3\,K\,mol^{-1}$ at 15 K, before

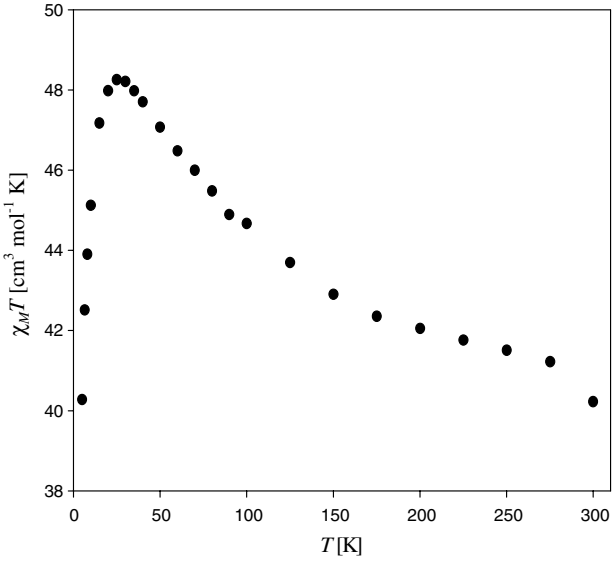

Fig. 5. Plot of $\chi_M T$ vs. T for complex **1** at 1 kG.

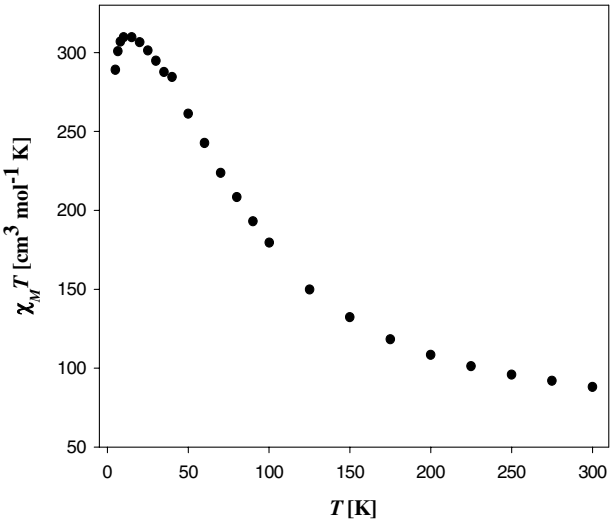

Fig. 6. Plot of $\chi_M T$ vs. T for complex **2** at 1 kG.

dropping to 289 cm^3 K mol^{-1} at 5.0 K. In each case the data suggest a very large ground state spin value. The final decrease of the $\chi_M T$ at the lowest temperatures is likely due to Zeeman effects and weak intermolecular exchange interactions. The 25 K peak value for complex **1** suggests an $S = 10$ spin ground state value, whereas the 15 K peak value for the Mn_{25} cation suggests either an $S = 49/2$ or 51/2 state, whose spin-only ($g = 2$) values would be 337.8 and 312.4 cm^3 K mol^{-1}, respectively.

In order to identify the ground states, magnetization (M) data in the 1.8–4.0 K and 0.1–7 T ranges were collected and fit by matrix diagonalization to a model that assumes only the ground state is populated, includes axial zero-field splitting ($D\hat{S}_z^2$) and Zeeman interactions, and incorporates a full powder average.

For complex **1**, we could not get an acceptable fit under any reasonable conditions, and we attribute this to the population of low-lying excited states, even at these low temperatures. For complex **2**, we used only low fields ($\leqslant$8 kG) to avoid problems associated with M_S levels from excited states with higher S values crossing with the ground state, which would lead to an erroneously high value for the ground state S. The fitting (solid lines in Fig. 7) of the magnetization data gave $S = 51/2$, $D = -0.021(1)$ cm^{-1}, and $g = 1.87(1)$. The fits for $S = 49/2$ and 53/2 were only slightly inferior, and on the basis of the magnetization fits alone, we therefore conclude that the ground state spin of **2** is $S = 51/2 \pm 1$.

An $S = 51/2$ ground state and negative D value suggested that **2** might have a sufficient barrier to magnetization relaxation to be an SMM. The upper limit to this barrier is given by $(S^2 - 1/4)|D|$ for a half-integer spin, or only 14.3 cm^{-1} for **2**, but the actual (or effective) barrier will be significantly less due to QTM through the barrier.

3.3.2. AC Magnetic susceptibility

AC susceptibility measurements were carried out on both samples in the 1.8–10 K temperature range to obtain reliable ground state spin values and assess whether the complexes might be SMMs. For complex **1**, no out-of-phase signal was observed whereas for complex **2** the presence of a frequency-dependent signal was observed below 3 K. The latter suggests **2** might be an SMM. The in-phase data extrapolated to 0 K indicate spin ground states of $S = 10$ and $S = 51/2$ for complexes **1** and **2**, respectively.

3.3.3. Single crystal magnetic measurements

The confirmation of possible SMM behavior requires the observation of hysteresis loops. Single crystals of **1** and **2** were therefore investigated using a micro-SQUID [21], and the obtained M versus applied DC field sweeps are shown in Figs. 8 and 9, respectively. Hysteresis loops, the diagnostic property of a magnet, were observed below ~0.7 K, their coercivities increasing with decreasing temperature, as expected for the superparamagnet-like properties of a SMM. The loops do not exhibit the step-like features indicative of QTM, but it is possible that steps are present but smeared out by broadening effects from dipolar and transverse fields, low-lying excited states, and/or a distribution of molecular environments. The low temperature at which both complexes are SMMs is clearly due to a small D value, which is consistent with the nearly perpendicular disposition of the Mn^{III} JT axes, the primary source of the molecular anisotropy.

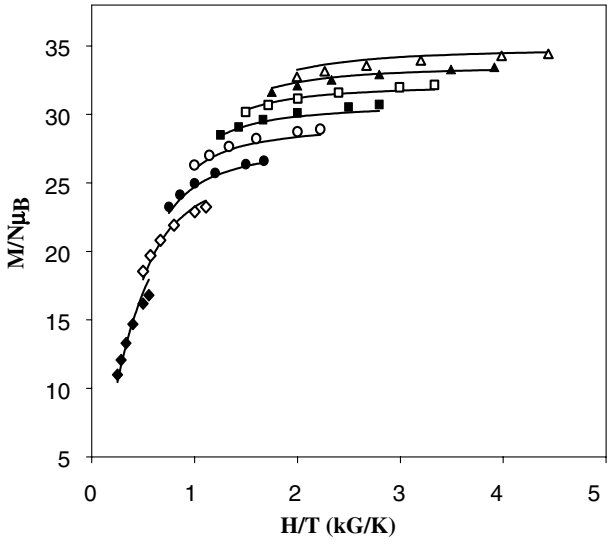

Fig. 7. Plot of reduced magnetization ($M/N\mu_B$) vs. H/T for **2** at 8 (△), 7 (▲), 6 (□), 5 (■), 4 (○), 3 (●), 2 (◇) and 1 (◆) kG. The solid lines are the fit; see the text for the fitting parameters.

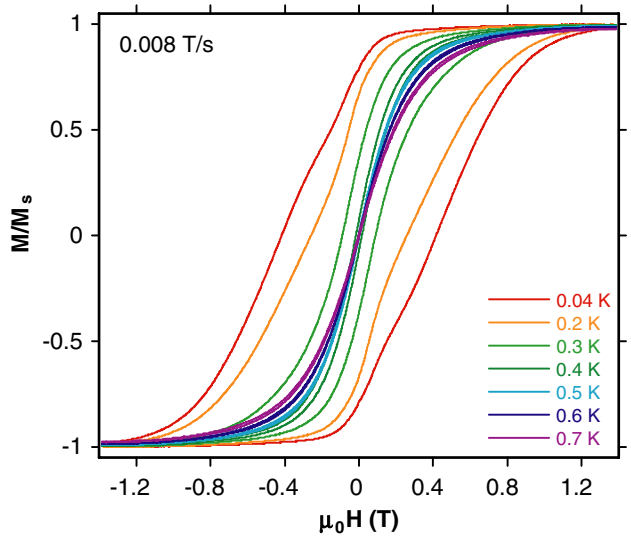

Fig. 8. Magnetization (M) vs. field ($\mu_0 H$) hysteresis loops for single crystals of **1** at the indicated temperatures.

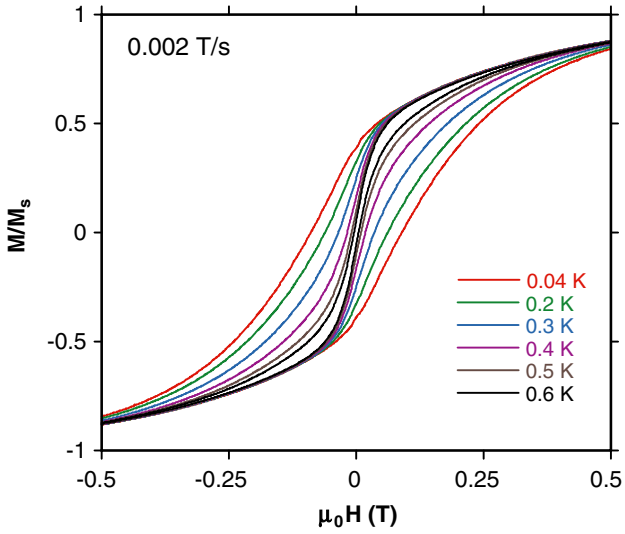

Fig. 9. Magnetization (M) vs. field ($\mu_0 H$) hysteresis loops for single crystals of **2** at the indicated temperatures.

4. Conclusions

A mixed chelate strategy has been used to synthesize two new SMMs $[Mn_{11}O_2(OH)_2(nmpd)(pdmH)_5(pdm)_5Cl_6]\cdot 4MeCN$ (**1**) and $[Mn_{25}O_{18}(OH)_2(N_3)_{12}(pdm)_6(pdmH)_6]Cl_2\cdot 12MeCN$ (**2**). Complexes **1** and **2** have novel core topologies containing seven Mn^{III} and four Mn^{II} ions for the former complex and one Mn^{IV}, eighteen Mn^{III} and six Mn^{II} ions for the latter. Both complexes are amongst the largest spin and size SMMs reported to date. Complex **2**, in addition to being the largest mixed-valent $Mn^{II}/Mn^{III}/Mn^{IV}$ cluster and the largest spin SMM to date, also has the largest spin ($S = 51/2$) for any molecular species, the same as that suggested for the cyano-bridged $Mn^{II}{}_9Mn^{V}{}_6$ complex [22].

5. Supplementary material

Crystallographic data have been deposited with Cambridge Crystallographic Data Centre, CCDC Nos. 238515 and 266403. Copies of this information may be obtained from The Director, CCDC, 12 Union Road, Cambridge, CB2 1EZ, UK (fax: +44 1233 336033; e-mail: deposit@ccdc.cam.ac.uk or www.ccdc.cam.ac.uk).

Acknowledgment

This work was supported by the National Science Foundation.

References

[1] G. Christou, D. Gatteschi, D.N. Hendrickson, R. Sessoli, MRS Bull. 25 (2000) 66, and references therein.
[2] R. Sessoli, H. Tsai, A.R. Schake, S. Wang, J.B. Vincent, K. Folting, D. Gatteschi, G. Christou, D.N. Hendrickson, J. Am. Chem. Soc. 115 (1993) 1804.
[3] E.K. Brechin, J. Yoo, M. Nakano, J.C. Huffman, D.N. Hendrickson, G. Christou, Chem. Commun. (1999) 783.
[4] J. Yoo, E.K. Brechin, A. Yamaguchi, M. Nakano, J.C. Huffman, A.L. Maniero, L.-C. Brunel, K. Awaga, H. Ishimoto, G. Christou, D.N. Hendrickson, Inorg. Chem. 39 (2000) 3615.
[5] M. Soler, W. Wernsdorfer, K. Folting, M. Pink, G. Christou, J. Am. Chem. Soc. 126 (2004) 2156.
[6] W. Wernsdorfer, N. Aliaga-Alcalde, D.N. Hendrickson, G. Christou, Nature 416 (2002) 406.
[7] D. Price, S. Batten, B. Moubaraki, K. Murray, Chem. Commun. (2002) 762.
[8] E.K. Brechin, C. Boskovic, W. Wernsdorfer, J. Yoo, A. Yamaguchi, C. Sanudo, T. Concolino, A. Rheingold, H. Ishimoto, D.N. Hendrickson, G. Christou, J. Am. Chem. Soc. 124 (2002) 9710.
[9] C. Boskovic, W. Wernsdorfer, K. Folting, J.C. Huffman, D.N. Hendrickson, G. Christou, Inorg. Chem. 41 (2002) 5107.
[10] N.E. Chakov, K.A. Abboud, L.N. Zakharov, A.L. Rheingold, D.N. Hendrickson, G. Christou, Polyhedron 22 (2003) 1759.
[11] J.T. Brockman, K.A. Abboud, D.N. Hendrickson, G. Christou, Polyhedron 22 (2003) 1765.
[12] M. Soler, W. Wernsdorfer, K.A. Abboud, J.C. Huffman, E.R. Davidson, D.N. Hendrickson, G. Christou, J. Am. Chem. Soc. 125 (2003) 3576.
[13] M. Soler, W. Wernsdorfer, K.A. Abboud, D.N. Hendrickson, G. Christou, Polyhedron 22 (2003) 1777.
[14] A. Morello, O.N. Bakharev, H.B. Brom, L.J. de Jongh, Polyhedron 22 (2003) 1745.
[15] E. Brechin, M. Soler, G. Christou, M. Helliwell, S. Teat, W. Wernsdorfer, Chem. Commun. (2003) 1276.
[16] C.J. Milios, C.P. Raptopoulou, A. Terzis, F. Lloret, R. Vicente, S.P. Perlepes, A. Escuer, Angew. Chem. Int. Ed. 43 (2004) 210.
[17] M. Murugesu, J. Raftery, W. Wernsdorfer, G. Christou, E.K. Brechin, Inorg. Chem. 43 (2004) 4203.
[18] M. Murugesu, W. Wernsdorfer, K.A. Abboud, G. Christou, Angew. Chem. Int. Ed. 44 (2005) 792.
[19] E.C. Sañudo, W. Wernsdorfer, K.A. Abboud, G. Christou, Inorg. Chem. 43 (2004) 4137.
[20] B. Pilawa, M.T. Kelemen, S. Wanka, A. Geisselmann, A.L. Barra, Europhys. Lett. 43 (1998) 7.
[21] W. Wernsdorfer, Adv. Chem. Phys. 118 (2001) 99.
[22] J. Larionova, M. Gross, M. Pilkington, H. Andres, H. Stoeckli-Evans, H. Gudel, S. Decurtins, Angew. Chem. Int. Ed. 39 (2000) 1605.